^{1}H NMR Cryoporometry Study of the Melting Behavior of Water in White Cement

Joanna Boguszyńska and Jadwiga Tritt-Goc

Institute of Molecular Physics, Polish Academy of Sciences,
ul. Smoluchowskiego 17, 60-179 Poznań, Poland

Reprint requests to Dr. J. T.-G.; E-Mail: jtg@ifmpan.poznan.pl

Z. Naturforsch. **59a,** 550 – 558 (2004); received April 23, 2004

The pore size of white cement samples is studied by the melting behaviour of water confined in it, using ^{1}H NMR cryopormetry. The influence of the preparing method and antifreeze admixture on the pore size and distribution in cement samples is investigated at 283 K. The addition of an antifreeze admixture [containing 1% Sika Rapid 2 by weight of the dry cement] influences the porosity. In wet prepared samples we observed a significant increase in the quantity of mesopores between 0.8 and 5 nm and a smaller increase of mesopores between 5 and 10 nm, when compared to cement without admixture. The compressive strength is related to the porosity of the cement. Therefore the cement with Sika Rapid 2, wet prepared at 278 K shows a higher strength than all other measured samples.

Key words: Cement; Sika Rapid 2; NMR; Melting; Porosity.

1. Introduction

The pore size and its distribution play an important role in the physical and chemical properties of porous media and are the most important criteria for the classification of these materials. Traditionally we distinguish macroporous materials having a pore diameter larger than 50 nm (capillary pores); mesoporous materials with pores in the range 2 to 50 nm (mesopores) and microporous materials with pores smaller than 2 nm (gel pores) [1]. However, some materials like cements are characterized by the whole range of pores cited above. The composition of the clinker, the water/cement ratio of the paste, the admixture used, the curing temperature, and the relative humidity are the parameters which determine the size and distribution of pores in cement.

Gas adsorption-desorption techniques [2] and mercury porosimetry [3] are the classical methods used in the determination of pore size. However, both methods are time consuming, and mercury porosimetry is a destructive technique which results in an irreversible damage of the investigated material. Another non destructive method used to determine the pore size and distribution is ^{1}H NMR cryoporometry [4 – 11]. The method relies on the fact that liquid confined within the pores of materials exhibits a melting point that is lower than the normal (bulk) melting point by a temperature difference that is inversely proportional to the pore diameter as given in the Gibbs-Thompson (Kelvin) equation

$$\Delta T_{\mathrm{m}} = T_{\mathrm{m}} - T_{\mathrm{m}}(r) = \frac{4\sigma T_{\mathrm{m}}}{r\Delta H_{\mathrm{f}}\rho}, \tag{1}$$

where T_{m} and $T_{\mathrm{m}}(r)$ are the melting point of the bulk and confined liquid, respectively, r is the pore radius of unconnected cylindrical pores, ρ the density of the crystal, σ the surface energy of the solid-liquid interface and ΔH_{f} the bulk enthalpy of fusion. The relation given by (1) derives from a classical thermodynamic approach [10 – 13] and appears to fit the experimental results presented here. However, all the theoretical approaches assume that the geometrical confinement of the fluid in the pore and not the strength of the fluid-wall interaction is important for the nucleation. A porous material filled with liquid, which is then cooled, will produce a distribution of melting temperatures that depends on the pore size distribution. Equation (1) can be rewritten as

$$\Delta T_{\mathrm{m}} = \frac{k}{r}, \tag{2}$$

where k is a constant characteristic for the liquid used to saturate the pores. For small pores (2) should be modified as

$$\Delta T_{\mathrm{m}} = \frac{k}{r - \lambda}. \tag{3}$$

In (3) λ is the thickness of the surface layer of the confined liquid, which further depresses the temperature of the melting/freezing transition [14–16]. Therefore, rather than sensing the pore radius r, the liquid confined in pores feels an effective pore radius, $r - \lambda$. For larger pores, where $r \gg \lambda$, (2) is satisfactorily accurate.

This paper presents the influence of the pore size and distribution on the melting transition of water confined in white cement and white cement with an antifreezing admixture studied by ^{1}H NMR cryoporometry. The influence of the preparing method (wet or dry) of the samples, and of the antifreeze admixture is shown. Water was used as a probe molecule to determine the pore size and distribution. Although there is no consensus as to the value of k in (1) for water confined in porous media, we use a value of 51.5 K nm based on the work by Schmidt et al. [6] on water confined in zeolite micropores. In our previous paper [7] we used the same value of k on water confined in cement paste.

The freezing/melting behaviour of water in cement is a fundamental problem, still not well understood. In addition, such studies have direct application because cement plays an important role in modern society. The hardened cement paste is the binding matrix in nearly all kinds of concrete. In most countries concrete is exposed to freezing temperatures, with resulting freezing damage. The public costs for concrete repair are enormous. Therefore it must be of common interest to obtain a better knowledge of the behaviour and properties of cement and to find the proper antifreeze admixture, which will modify the properties of cement. Such modified cement can be used in the construction industry at lower temperatures (below 283 K) without lowering the quality of the buildings.

The compressive strength developments as function of the preparing method of white cement, and white cement with antifreeze admixture were also studied, and the results are presented in this paper.

2. Experimental

2.1. Sample Preparation

The melting behaviour of water in 6 months old white cement, without and with an antifreeze admixture [containing 1% Sika Rapid 2 by weight of the dry cement] which went through a wet or dry curing process at 278 K, was investigated. For dry curing the cement samples were placed in open glass vials, for wet curing they were placed in tightly sealed plastic bags, with water-soaked cotton, which guaranteed 100% humidity. The samples were prepared at a water-to-cement ratio (w/c) of 0.4. The cement was supplied by AALBORG PORTLAND POLAND, the antifreeze admixture Sika Rapid 2 by SIKA POLAND.

Table 1. Composition of white cement (courtesy AALBORG PORTLAND POLAND).

Compund	Percent
Tricalcium silicate (C_3S)	72
Dicalcium silicate (C_2S)	18
Tricalcium aluminate (C_3A)	4.5
Tetracalcium aluminoferrite (C_4AF)	1.0

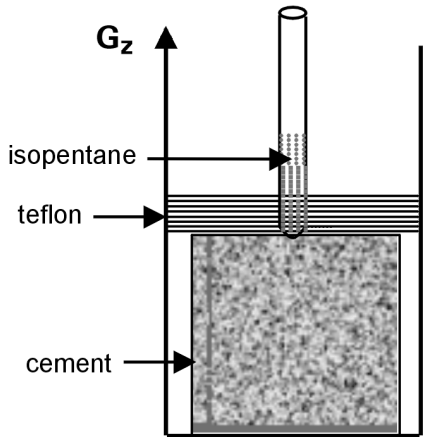

Fig. 1a. The setting of the probe for the ^{1}H NMR measurements in the one-dimensional ^{1}H Single Point Imaging (1D ^{1}H SPI) measurements, showing also the direction of the applied gradient G_z.

White cement was chosen in order to reduce the influence of paramagnetic centres normally present in commercial cements, which reduce the NMR spin-spin relaxation time T_2 and lead to broad NMR absorption lines. For the composition of the white cement used in our experiments see Table 1.

For the NMR experiments cylindrical samples of approximately 0.8 cm diameter and 1 cm length (Fig. 1a) were prepared from either dry cement or dry cement with Sika Rapid 2. The samples were saturated with water and put into glass tubes. The tubes were then closed with Teflon corks containing a capillary with isopentane. The NMR signal from isopentane was used as reference, because its freezing point lies well below that of the lowest freezing point of water in the pores.

2.2. NMR Measurement Procedures

The ^{1}H NMR experiments were performed at 7.1 T on a Bruker AVANCE 300 spectrometer. The ^{1}H mea-

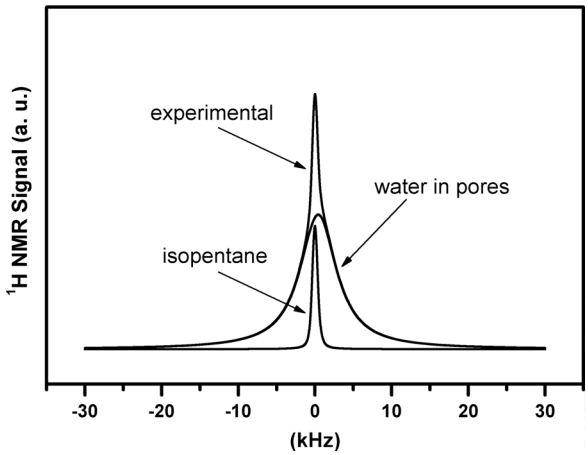

Fig. 1b. Examples of the spectrum obtained for water protons confined in pores of white cement at 251 K. Also the signal from isopentane, which serves as the calibration signal, is seen.

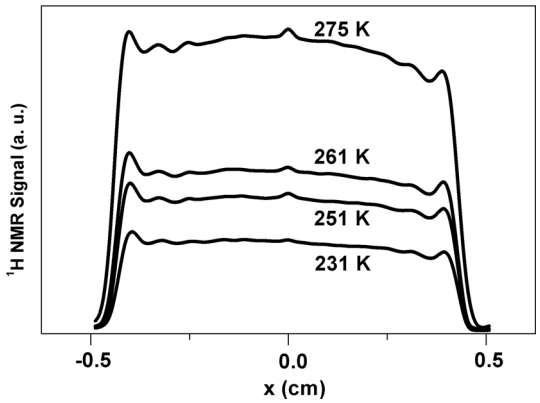

Fig. 1c. Examples of 1D profiles of the water protons confined in pores of white cement as functions of temperature.

surements were carried out with a 15 mm probehead. The temperature of the sample was regulated and stabilized to within ± 1 K with a Bruker VB-VT 1000/R temperature control unit using a flow of cold nitrogen. Each sample was first cooled until the liquid was frozen. Then the samples were warmed slowly, while measuring the NMR signal from the nonfrozen water only, until all the ice was melted. To reduce the chance of cracking of the hard cement paste, the temperature change was kept at 4 K/h and the sample was temperature equilibrated for 15 min at each temperature before any measurements were performed. Since supercooling is a common phenomenon, the measurements were made on raising the temperature after freezing the liquid to ca. 200 K.

The ^{1}H free-induction decay signal at each temperature was measured 30 μs after the 90° pulse. Because the T_2 of ice is about 6 μs, the magnetization of the ice protons will have decayed completely after 30 μs, while the decay of the magnetization corresponding to the nonfrozen water will be negligible. This ensures that only the signal from nonfrozen water will be measured. The ^{1}H NMR spectrum at 251 K is presented in Fig. 1b – solid line. Each of the measured signals was decomposed with an appropriate fitting procedure to two signals: one from nonfrozen water within the pores of the studied sample, and the second from isopentane. The normalized intensity data of the signal from nonfrozen water were then used to calculate the pore size distribution of the investigated cement sample.

In addition to the ^{1}H NMR signal, also the one-dimensional ^{1}H Single Point Imaging (1D ^{1}H SPI) profiles of the nonfrozen water filling the pores were acquired. The SPI MRI method has been proved to be the ideal method for imaging the hard cement samples [17 – 19]. 1D SPI experiments were performed with the phase encoding time $t_p = 110$ μs and the repetition time TR = 50 ms. The phase- encoding gradient G_z was applied in the *z* direction in 128 steps up to a maximal value of 0.93 T/m. The orientation of the phase-encoding gradient is shown in Figure 1a. Fourier transform of the phase-encoding signal produced profiles (the projection of the proton density in the studied sample in the direction of the phase- encoding gradient) with a resolution of 158 μm. Examples of the 1D profile for white cement at chosen temperatures are shown in Figure 1c. The homogeneous distribution of water within the sample and the increase of the intensity of the signal with the temperature, due to the melting of the water within the pores, are easily seen. The profile of the reference signal is not shown in Figure 1c. Since the spin–spin relaxation time of ice and adsorbed water are orders of magnitude shorter than that of pore water, no significant NMR signal can be observed from these two phases with the above chosen encoding times. This allows a quantitative investigation of the amount of liquid water within the cement paste as a function of temperature.

The programs XWIN – NMR 2.6 and Para Vision 2.1 were used for the spectroscopic and imaging experiments, respectively.

2.3. Compressive Strength Measurements

Compressive strength measurements were performed on a hydraulic compressive testing apparatus,

by PN–EN 196–1 norm (polish norm for compressive strength measurements). Test samples: white cement, wet and dry prepared at 278 K, without and with an antifreeze admixture [containing 1% Sika Rapid 2 by weight of the dry cement]. Shape: cylindrical, approximately 1.8 cm in diameter and 1.8 cm long. Age: 1, 2, 3, 7 and 28 days. Compressive strength testing was performed on three specimens of every sample. The average strength is reported.

3. Theory

The liquid in a pore solidifies at a lower temperature then the free liquid. The decrease of the freezing temperature depends on the size of the pore, the properties of the liquid and the interaction between the liquid and the material constituting the surface of the pore. In our study the pores were relatively large, and the latter interaction had a negligible effect on the freezing temperature.

Applying the NMR method to evaluate the pore size distribution relies on the different intensities of the FID signals arising from the nonfrozen and frozen liquid. In a typical experiment of that kind the FID from the frozen liquid (in our case ice) is very short and with proper setting of the NMR spectrometer is not observed. Therefore the intensity of the FID signal is proportional to the amount of nonfrozen liquid in all pores of the studied sample.

The relation between the intensity of the NMR signal and the inverse temperature of the liquid was derived as (6) in [6] and later rewritten by Aksnes et al. [11] in the form

$$I(X) = \sum_{i=1}^{N} I_{0i}[1 - \mathrm{erf}\{(X - X_{ci})/(\sqrt{2}\sigma_i)\}]/2 \quad (4)$$

with

$$\mathrm{erf}(Z) = \frac{2}{\sqrt{\pi}} \int_0^Z \exp(-u^2)\mathrm{d}u, \quad (5)$$

where I_{0i} represents the intensity of the NMR signal from the liquid in the i-th type (size) of pores, N is the number of phase transitions liquid-solid and is equivalent to the number of distinctively different pore size containing the studied liquid, $X = 1000/T$, where T is the absolute temperature in Kelvin, $X_{ci} = 1000/T_{ci}$, where T_{ci} is the temperature of the liquid-solid phase transition for the i-th type of pore, $\sigma_i = 1/\Delta T$ is the width of the phase transition for the I-th type of pore.

For the purpose of numerical calculation we rewrite (4) into the form

$$I(X) = \sum_{i=1}^{N} I_{0i}/2 - \sum_{i=1}^{N} I_{0i}\mathrm{erf}\{(X - X_{ci})/(\sqrt{2}\sigma_i)\}/2 \quad (6)$$

and denote the first term after the equal sign by C. The value of C may be arbitrary but should be large enough to assure a positive value of *I(X)*, as such a condition simplifies the calculation. In our studies C was set to 17. Since the final values of *I(X)* were always normalized to 1.0, the value of C has no effect on the final results.

The fitting of parameters in (6) to the experimental data was done with a computer program written in Fortran90. Our FORTRAN compiler has no standard intrinsic erf() function, therefore we wrote a subroutine calculating it. A series expansion of erf() function was used. To check the accuracy of this subroutine, we calculated the erf() function values on the CRAY SV1 computer in the Poznań Supercomputing and Networking Center (http://www.man.poznan.pl/resources/index.html), as the error function is a standard intrinsic function in the Fortran compiler. These calculated values of the erf() function were equal to six significant digits to the values obtained with our subroutine, which is completely satisfactory for the purpose of our analysis.

The computer program was designed to permit fitting of up to 10 sets of parameters (I_{0i}, X_{ci}, and σ_i). The quality of the fit was measured by calculating

$$\Delta F = \frac{1}{P} \sum_{m=1}^{P} \left[\frac{I_{\mathrm{ex}}(X_m) - I_{\mathrm{cal}}(X_m)}{I_{\mathrm{ex}}(X_m)} \right]^2, \quad (7)$$

where P denotes number of experimental points, the subscript ex stands for experimental and cal for calculated values of the FID intensities, respectively.

With such a large number of fitted parameters there is a great probability of falling into a local minimum, when fitting is done with automatic changing of parameters. To avoid such a trap, our program was designed for manual changes of fitted parameters, and some experience of the researcher allows a very efficient minimizing of ΔF values given in (7). The program itself for Intel based computers is available upon request.

The melting point distribution curve, $\mathrm{d}I/\mathrm{d}X$ vs. X, we obtained by differentiating (6) with respect to X.

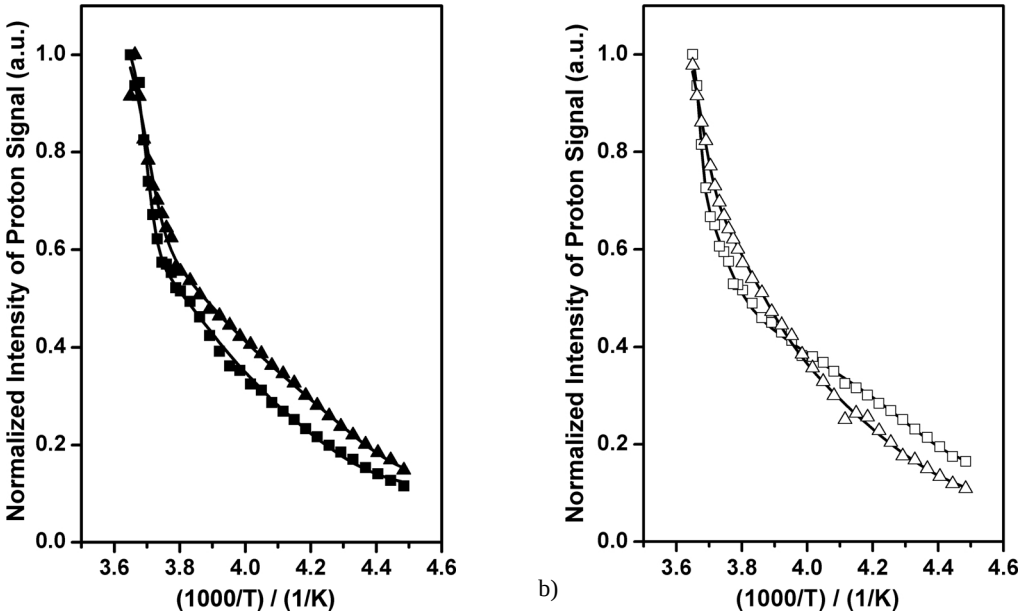

Fig. 2. ^{1}H NMR signal intensity vs. inverse of temperature of water enclosed in the pores of (a) white cement, sample *Wa* (solid squares) and white cement with Sika Rapid 2, sample *Wb* (solid triangles) and (b) white cement (open squares), sample *Da* and white cement with Sika Rapid 2, sample *Db* (open triangles). The solid lines represent the best fits to the experimental data using (6). The samples were hydrated in constant wet (*samples W*) and dry (*samples D*) conditions, respectively.

The curve is a sum of Gaussian functions [6]:

$$\frac{\mathrm{d}I}{\mathrm{d}X} = \sum_{i=1}^{N} \frac{I_{0i}}{\sqrt{2\pi}\sigma_i} \exp\left[-\left\{ \frac{X - X_{ci}}{\sqrt{2\sigma_i}} \right\}^2 \right]. \qquad (8)$$

An analytical function describing the pore size distribution $\mathrm{d}I/\mathrm{d}r$ vs. r, is easily obtained from (4) and (8):

$$\frac{\mathrm{d}I}{\mathrm{d}r} = \qquad (9)$$

$$\sum_{i=1}^{N} \frac{I_{0i}}{10^3 k\sqrt{2\pi}\sigma_i} \left(XT_\mathrm{m} - 10^3\right)^2 \exp\left[-\left\{ \frac{X - X_{ci}}{\sqrt{2\sigma_i}} \right\}^2 \right].$$

4. Results and Discussion

The key parameter of our NMR measurements, which serves to determine the pore size and distribution in cement samples is the intensity of the NMR signal from pore water. Figures 2a and 2b show the ^{1}H NMR signal intensity of water confined in cement samples, as a function of the inverse temperature. For simplicity we will identify the cement samples prepared in wet and dry conditions as *W* and *D*, respectively. In our set of the samples we will denote the white cement samples as *Wa* and *Da*, and the white cement with Sika Rapid 2 additive will be named *Wb* and *Db*. The symbols in Figs. 2a and 2b represent the experimental data.

The melting behaviour of water confined in the pores was measured up to the room temperature. The intensities of the signal were constant above 273 K but some scatter over the average value was observed. Therefore we used for the fitting procedure only the experimental data below 273 K which is justified by the fact that the freezing/melting behaviour of water confined in pores is observed only below this temperature. The smooth increase in the intensity of the ^{1}H NMR lines with increasing temperature, easily seen in Figs. 2a and 2b, is the result of the gradual melting of the frozen water within the cement paste. This suggests a nearly continuous distribution of the pore sizes within the samples.

The solid lines in Fig. 2a (wet preparing) represent 5-phase fits and in Fig. 2b (dry preparing) 4-phase fits to the experimental data using (6). A 4-phase fit for wet prepared samples (not shown in the figure) was also carried out, but it produces less satisfactory experimental data. For dry prepared samples the 5-phase and the 4-phase fits gave the same results, as seen by

Sample	The values of the fitting parameters					
	i	I_{0i}	T_{ci}/K	X_{ci}/K^{-1}	σ_i/K^{-1}	r/nm
	1	2,00	271,0	3.6	0,033	23,84
Sample *Wa*	2	3,98	269,3	3.71	0,281	13,34
white cement (wet)	3	0,17	260,5	3.84	0,200	4,07
	4	0,31	237,8	4.21	0,095	1,46/1.81
	5	0,27	228,4	4.38	0,061	1,15/1.50
	1	0,48	271,5	3.68	0,112	31,02
Sample *Wb*	2	2,00	270,2	3.7	0,044	17,4
white cement/Sika Rapid 2 (wet)	3	3,04	260,6	3.84	0,293	4,10
	4	0,54	235,1	4.25	0,200	1,35/1.70
	5	0,46	228,8	4.37	0,127	1,16/1.51
	1	1,46	272,3	3.67	0,012	59,88
Sample *Da*	2	2,21	270,2	3.7	0,083	17,4
white cement (dry)	3	2,49	247,7	4.04	0,353	2,02
	4	0,30	230,5	4.34	0,090	1,21/1.56
	1	1,64	271,9	3.68	0,034	40,87
Sample *Db*	2	2,44	264,7	3.78	0,153	6,09
cement/Sika Rapid 2 (dry)	3	2,51	248,7	4.02	0,250	2,10
	4	0,49	235,8	4.24	0,169	1,38/1.73

Table 2. Numerical values obtained by fitting (6) to the experimental data: the relative intensity (I_{0i}), the inverse transition temperature (X_{ci}), the width of the phase transition for the i-th type of pore σ_i and the pores radius (r) calculated using (2) or (3).

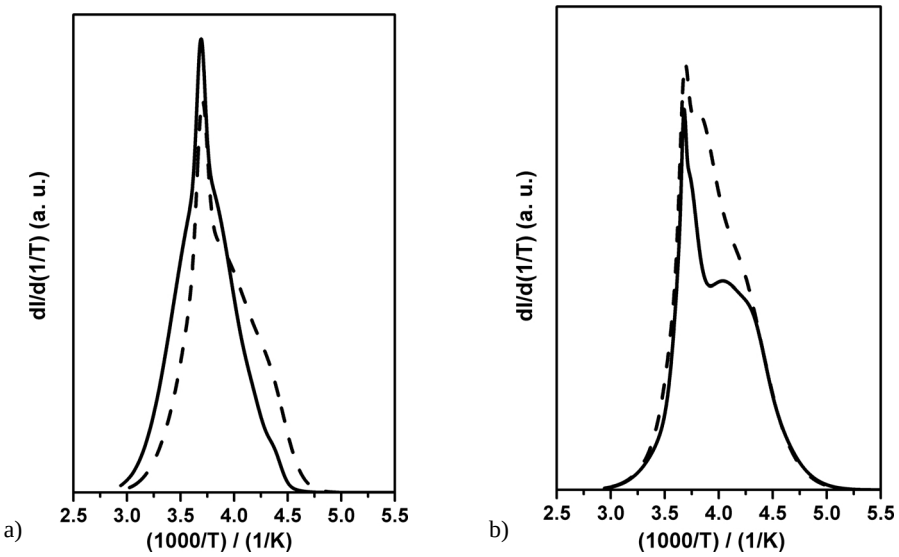

Fig. 3. Melting point distribution curves derived from (8) for water confined in pores of (a) white cement, sample *Wa* (solid line) and white cement with Sika Rapid 2, sample *Wb* (dashed line) and (b) white cement, sample *Da* (solid line) and white cement with Sika Rapid 2, sample *Wb* (dashed line). The samples were hydrated in constant wet (*samples W*) and dry (*samples D*) conditions, respectively.

the naked eye. However, the function ΔF given by (7), which measure the quality of the fit, is smaller for the 4-phase than for the 5-phase; therefore the 4-phase fit was chosen as the better one.

Numerical values of the relative intensity I_{0i}, and the width σ_i of the phase transition for the i-th type of pore obtained by fitting (6) to the experimental data, are presented in Table 2. The values of ΔF for all fitted curves are between 0.31×10^{-3} and 0.81×10^{-3}. Equation (6) was derived with the assumption of a log-normal distribution of the correlation time of the confined molecules [3]. The excellent agreement between experiment and theory, presented in Figs. 2a and b, support this assumption. Using (2), we relate the melting point depression ΔT_{m} (for every inverse transition temperature (X_{ci}) listed in Table 2) of water enclosed in a pore to the radius r of the pore. The obtained values of r are listed in Table 2. For lowest values of the tran-

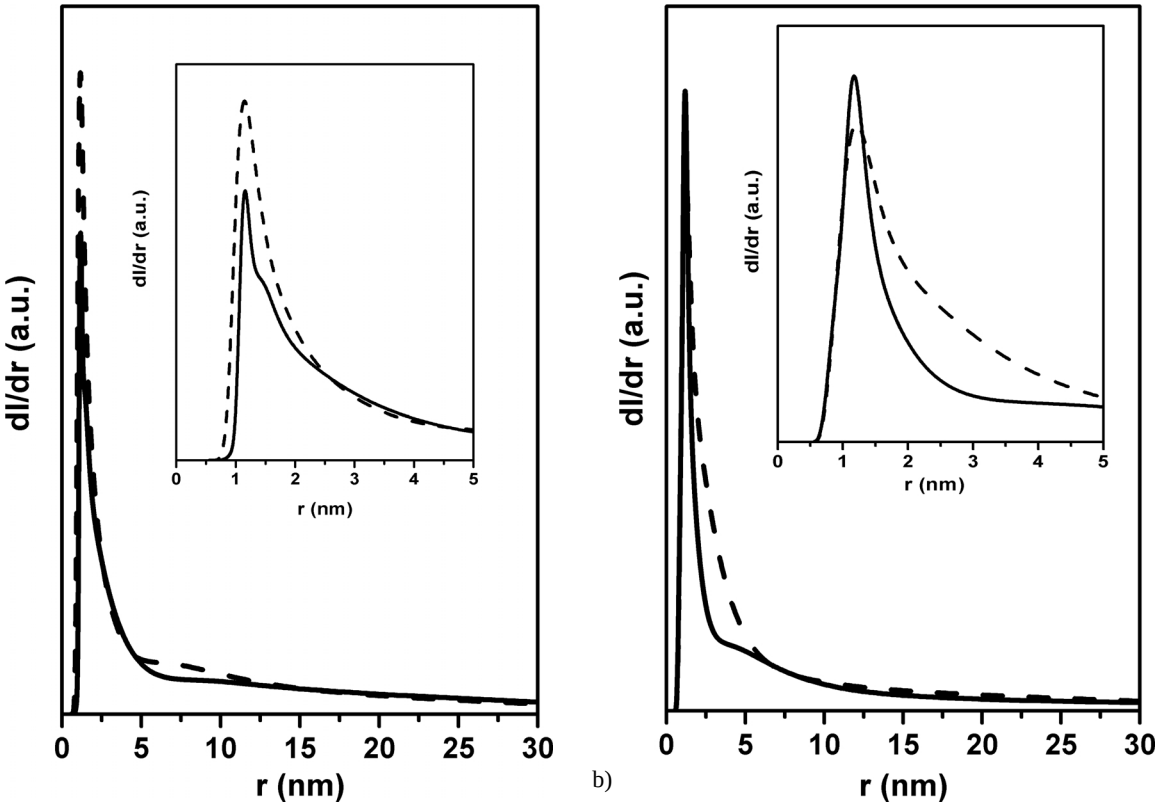

Fig. 4. Pore size distribution curves derived from (9) for water confined in pores of (a) white cement, sample *Wa* (solid line) and white cement with Sika Rapid 2, sample *Wb* (dashed line) and (b) white cement, sample *Da* (solid line) and white cement with Sika Rapid 2, sample *Db* (dashed line). The inset shows the distribution of smaller pores for the samples. The samples were hydrated in constant wet (*samples W*) and dry (*samples D*) conditions, respectively.

sition temperatures (X_{ci}) two values of r are cited. The second one was calculated with (3) taking into account the thickness of the surface water $\lambda = 0.35$ nm. The parameter $\lambda = 0.35$ nm was given by Schmidt et al. [6] who derived the melting point of ice in five MCM-41 materials with pore radii in the range 1.0 – 2.0 nm, using an NMR technique. At larger pore radii the size of the nonfreezing surface layer is much smaller than the pore radius, and (3) can be approximated by (2).

The melting point distribution curves for samples *W* and samples *D* are presented in Figs. 3a and b, respectively. The solid lines represent the white cement samples and the dashed lines the cement with Sika Rapid 2 ones. The curves were calculated by inserting the fitted I_{0i}, X_{ci}, and σ_I values from Table 2 into (8). The temperature transition point (X_{c1}), corresponding to the inverse temperature at first maximum of the melting point distribution curve (see Figs. 3a and b) is interpreted as the average depressed melting point of the confined substance, in our case water, in accordance with the Gibbs-Thompson relationship.

Slightly larger transition widths at the lowest temperature observed for sample *Wb* when compared to sample *Wa*, indicate a slightly higher heterogeneity in the structure of sample *Wb*.

The pore size distribution curves (dI/dr) for the four studied samples obtained from (9) using the melting point distribution curves from Figs. 3a and b are presented in Figs. 4a and b, respectively. Using the ^{1}H NMR cryoporometry method and water as probe molecules, a maximum pore radius of 50 nm can be determined accurately. This is due to the fact that the maximum pore size that can be determined using this technique, depends on the temperature resolution during the measurements. In our experiment a maximum temperature resolution of 1 K was achieved. The curves in Fig. 4a and b reveal a quite broad pore distribution centered around 1.5 nm. However, the pore

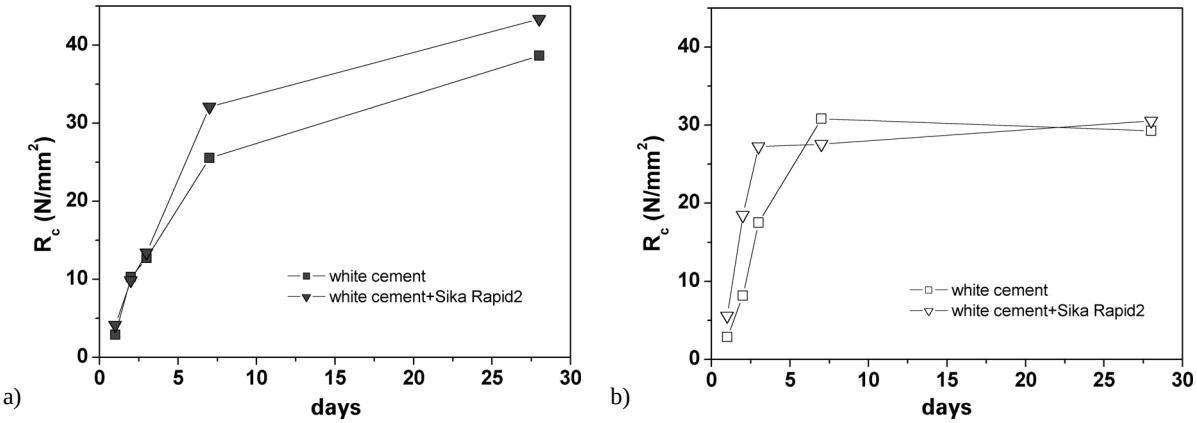

Fig. 5. Compressive strength development of (a) white cement, sample *Wa* (solid squares) and white cement with Sika Rapid 2, sample *Wb* (solid triangles) and (b) white cement, sample *Da* (open squares) and white cement with Sika Rapid 2, sample *Db* (open triangles). The samples were hydrated in constant wet (*samples W*) and dry (*samples D*) conditions, respectively.

size distributions determined for the white cement with Sika Rapid 2 samples (samples *Wb* and *Db*) are broader than those for the white cement samples (sample *Wa* and sample *Da*). The distribution curve for sample *Wb* is broader in the range of small mesopores (0.8 – 2 nm) than for sample *Wa*. For sample *Db* (dry preparing) the broadening is more significant and occurs at larger pore sizes (1.5 – 5 nm). The increase in the quantity of smallest mesopores 0.8 to 2.5 nm and of pores with radii between 5 to 10 nm in white cement with Sika Rapid 2 (sample *Wb*) when compared to the sample *Wa* is observed in Figure 4a. In Figure 4b, a significant increase in the quantity of pores is only seen with radii of 1 to 5 nm.

Figure 5a and b show the compressive strength development as a function of preparation age for the samples *W* and *D*, respectively. For wet prepared samples – Fig. 5a, two observations can be noted: (a) adding the antifreeze admixture of 1% Sika Rapid 2 by weight of the dry cement has no influence on the compressive strength at an early age; (b) Sika Rapid 2 additive produced higher strength improvement after 3 days of preparation. As a result, the compressive strength of a cement sample with antifreeze admixture after 28 days (43.4 N/mm^2) is by 13% higher than that of white cement (38.4). For dry preparation samples (Fig. 5b), the addition of Sika Rapid 2 to the cement results in an increase of the compressive strength at an early age, but after 28 days both samples have the same strength of about 30 N/mm^2. A comparison of the final measured values of the compressive strength for wet and dry prepared samples (Fig. 5a and b) lead to the conclusion about the positive influence of antifreeze admixture in case of wet prepared cement. The compressive strength obtained for the wet prepared sample with admixture is about 45% higher when compared to the compressive strength measured for dry prepared samples.

5. Conclusion

In this study, the influence of the preparing condition and antifreeze admixture on the pore size and distribution in cement samples was investigated. Based on these experimental results, it can be concluded that Sika Rapid 2 admixture influences the porosity. Addition of an antifreeze admixture [containing 1% Sika Rapid 2 by weight of the dry cement] results, in wet prepared samples, in a significant increase in the quantity of mesopores between 0.8 and 5 nm and a smaller increase of mesopores between 5 and 10 nm when compared with the cement without admixture. The compressive strength is related to the porosity of the cement. Therefore the cement with Sika Rapid 2, wet prepared at 278 K shows the highest strength of all measured samples.

The smaller strength observed for dry prepared samples can be explained as follows. When the cement is hydrated in dry conditions then a fast evaporation of the water from the cement paste occurs. The larger pores contain partially no water and can't be filled with the products of the hydration reaction which takes place with time. This results in larger pores being left in the final material. Thus, the cement hydrated in dry conditions is characterized by the worst technical pa-

rameters. The results of our measurements agree with this statement.

The ^{1}H NMR cryporometry used in our measurements is well suited for studying cement despite of the fact that the pore characteristics in cement are rather complex due to the irregularities and interconnections of pores. We have shown that this method is able to detect even small changes in the size and distribution of pores in the range 1 to 50 nm. In this study we have shown the influence of the preparation conditions and admixture added to the cement paste hydrated at 278 K. The studies are continued and will be presented in the next paper.

Acknowledgement

Authors would like to thank to Dr. Roman Goc from the A. Mickiewicz University for help in the numerical calculations and Mrs. G. Gramza from Technical University of Poznan for technical assistance in the compressive strengths measurements.

[1] H. F. W. Taylor, Cement Chemistry, Academic Press, New York 1990.
[2] K. S. W. Sing, D. H. Everett, R. A. W. Haul, L. Moscou, R. A. Pierotti, J. Rouquerol, and T. Siemieniewska, Pure Appl. Chem. **57**, 603 (1985).
[3] S. J. Gregg and K. S. W. Sing, Adsorption, surface Area and Porosity, Academic Press, New York 1992, 2nd Edn.
[4] K. Overloop and L. Van Gerven, J. Magn. Reson., Ser. A. **101**, 179 (1993).
[5] D. Akporiaye, E. W. Hansen, R. Schmidt, and M. Stöcker, J. Phys. Chem. **98**, 1926 (1984).
[6] R. Schmidt, E. W. Hansen, M. Stöcker, D. Akporiaye, and O. H. Ellestad, J. Amer. Chem. Soc. **117**, 4049 (1995).
[7] R. Holly, J. Tritt-Goc, N. Piślewski, C. M. Hansson, H. Peemoeller, J. Appl. Phys. **88**, 7339 (2000).
[8] J. B. W. Webber, J. H. Strange, J. C. Dore, Magnetic Resonance Imaging **19**, 395 (2001).
[9] R. Valiullin and I. Furo, J. Chem. Phys. **116**, 1072 (2001).
[10] J. H. Strange, M. Rahman, and E. G. Smith, Phys. Rev. Lett. **71**, 3589 (1993).
[11] D. W. Aksnes, K. Forland, and L. Kimtys, Phys. Chem. Chem. Phys. **3**, 3203 (2001).
[12] K. M. Unruh, T. E. Huber, and C. A. Huber, Phys. Rev. B **48**, 9021 (1993).
[13] J. Warnock, D. D. Awschalom, and M. W. Shafer, Phys. Rev. Lett. **57**, 1753 (1986).
[14] H. A. Resing, J. K. Thompson, and J. J. Krebs, J. Phys. Chem. **68**, 1621 (1964).
[15] R. J. Pearson and W. Derbyshire, J. Colloid Interface Sci. **96**, 232 (1974).
[16] S. Stapf, R. Kimmich, and J. Niess, J. Appl. Phys.**75**, 529 (1994).
[17] M. Bogdan, B. J. Balcom, T. W. Bremner, and R. L. Armstrong, J. Magn. Reson A.**116**, 266 (1995).
[18] S. D. Beyea, B. J. Balcom. T. W. Bremner, P. J. Prado, A. R. Cross, R. L. Armstrong, and P. E. Grattan-Bellew, Solid State Nucl. Magn. Reson.**13**, 93 (1998).
[19] T. Nunes, E. W. Randall, A. A. Smoilenko, P. Bodart, and G. Feio, J. Phys. D: Appl. Phys. **29**, 805 (1996).